

Interdigitated Back-Contacted Carbon Nanotube–Silicon Solar Cells

Yuhua Bai, Qing Gao, Bingbing Chen, Wenheng Li, Xuning Zhang, Dehua Yang, Xueliang Yang, Jun Yan, Jingwei Chen, Jianming Wang, Dengyuan Song, Shufang Wang, Han Li, Benjamin S. Flavel, and Jianhui Chen*

Carbon/silicon heterojunctions provide a new perspective for silicon solar cells and in particular those made from carbon nanotubes (CNTs) have already achieved industrial-level power conversion efficiency and device size when using organic passivation and a back-junction design. However, the current state of the art device geometry for silicon photovoltaics is the interdigitated back contact (IBC) cell and this has yet to be demonstrated for CNT/Si solar cells due to the complexity of fabricating the required patterns. Herein, IBC-CNT solar cells are demonstrated via the simple spin coating of a conductive hole-selective passivating film and the evaporation of buried silicon oxide/magnesium electron-selective contacts for both polarities. The CNT coverage area fraction (f_{CNT}) and the gap between the two polarities are optimized to minimize electrical shading loss and ensure high photocarrier collection. Large-area (4.76 cm^2) highly efficient (17.53%) IBC-CNT solar cells with a V_{oc} of 651 mV and J_{sc} of 40.56 mA cm^{-2} are demonstrated and are prepared with one alignment step for the CNT/Si contact, and photolithographic-free and room-temperature processes. These performance parameters are among the best for solution-processed dopant-free IBC schemes and indicate the feasibility of using low-dimensional carbon materials in IBC solar cells.

cells include crystalline silicon (c-Si) solar cells,^[2] copper indium gallium selenide (CIGS) solar cells,^[3] perovskite solar cells,^[4–6] and dye-sensitized solar cells,^[7,8] which featured p-n homojunction and an efficient absorber. However, in the current photovoltaic industry, Si heterojunction (HJ) solar cells with an amorphous Si (a-Si) passivation layer on c-Si wafers are a promising carbon neutral technology.^[9] Using the most advanced interdigitated back contact (IBC) geometry design, the a-Si/c-Si HJ solar cell has achieved the highest efficiency of 26.7%,^[10] and it can also serve as the bottom cell in a stack with perovskite solar cells to efficiencies exceeding 30%.^[11] HJ solar cells largely rely on the use of boron- or phosphorus-doped Si for a “Si/Si” p-n junction, and this is associated with technological complexities and expensive vacuum equipment,^[12] which hinder its widespread industrialization. Thus, researchers have been seeking simplified solutions such as the so-called dopant-free alternatives such as transition metal oxides,^[13–16] organic films,^[17–20] and low-dimensional layers.^[21] It is within this family of materials that carbon nanomaterials have attracted extensive attention due to the formation of high-efficient carbon/silicon (C/Si) HJs.^[22–24]

1. Introduction


The development of high-efficiency solar cells will be key to reduce the carbon footprint of human activities on this planet and achievement of carbon neutrality.^[1] High-efficiency solar

Y. Bai, Q. Gao, B. Chen, W. Li, X. Zhang, D. Yang, J. Yan, J. Chen, S. Wang, J. Chen
Advanced Passivation Technology Lab
College of Physics Science and Technology
Hebei University
Baoding 071002, China
E-mail: chenjianhui@hbu.edu.cn

Y. Bai, Q. Gao, B. Chen, W. Li, X. Zhang, D. Yang, X. Yang, J. Yan, J. Chen, J. Chen
Province-Ministry Co-Construction Collaborative Innovation Center of Hebei Photovoltaic Technology
College of Physics Science and Technology
Hebei University
Baoding 071002, China

J. Wang, D. Song
R&D Department
Das Solar Co., Ltd.
No 43 Bailing South Road, Quzhou Green Industry Clustering Zone,
Quzhou, Zhejiang Province 324022, China

H. Li, B. S. Flavel
Institute of Nanotechnology
Karlsruhe Institute of Technology
Hermann-von-Helmholtz-Platz 1, 76344 Eggenstein-Leopoldshafen,
Germany

 The ORCID identification number(s) for the author(s) of this article can be found under <https://doi.org/10.1002/sstr.202200375>.

© 2023 The Authors. Small Structures published by Wiley-VCH GmbH. This is an open access article under the terms of the Creative Commons Attribution License, which permits use, distribution and reproduction in any medium, provided the original work is properly cited.

DOI: 10.1002/sstr.202200375

The C/Si HJs provide new perspectives for future solar cells due to features such as a tuneable band structure (metallic or semiconductor properties),^[25,26] multiple exciton generation,^[27–29] wide spectral absorption,^[30–32] and the high carrier mobility^[33–35] of carbon nanomaterials. Furthermore, C/Si HJs can be fabricated at room temperature with vacuum-free equipment and in environmentally friendly and potentially cost-effective ways. Various carbon materials have been studied for this purpose and include fullerenes (e.g., C₆₀), carbon nanotubes (CNTs), graphene, graphene oxides, and others [amorphous carbon (a-C)].^[36–39] However, it is the use of CNTs due to either metallic or semiconducting nature, widely tunable properties, and contacting Si with a high built-in potential that have gained significant interest.^[40–43]

CNT/Si HJ solar cells began with a window-like structure to define the active area and later progressed to industrial geometries. The first report of this technology was in 2007 by Wei et al. who demonstrated a 0.49 cm² device with a power conversion efficiency (PCE) of 1.4%.^[44] The geometry of Wei et al. allowed for a CNT film to be processed separately and then transferred to a window in the middle of the device. This design also made experiments with various chemical dopants easier. Following this preliminary work, the research field was witness to a rapid increase in PCEs, but until recently they have remained <18% and the device design faced problems with scale up and the device area remained small to 0.009–1 cm².^[40,45–49] The device design also lacked interface passivation due to the inability to grow traditional passivation layers like a-Si:H or SiN_x from

chemical vapour deposition (CVD) into interface. In our recent work, a passivation scheme involving organic thin films and a CNT ink was developed and this increased the efficiency up to >23% and was used to realize industrial size (245.71 cm²) device.^[50–52] However, despite the efficient and scalable breakthrough, the geometry used was still not state of art. The currently state of art device geometry in photovoltaics is IBC cell structure, where the emitter and contact are on the back of the wafer. This design provides numerous advantages over conventional geometries, including zero optical shading, independent control for optimum optical performance in the illuminating front side, and optimum electrical performance with simpler interconnection techniques on the backside, consequently higher efficiencies and improved esthetics.^[53–55] Therefore, in this work, we investigate a IBC-CNT/Si HJ solar cell design, which featured a conductive hole-selective passivating contact made from a CNT ink and buried silicon oxide/magnesium (SiO₂/Mg) electron-selective contact (ESC) for both polarities.

Figure 1 shows the schematic diagram of the IBC-CNT HJ solar cell. The fabrication process was simple and involved only five steps: wet chemical processing, front indium tin oxide (ITO)/a-Si:H deposition by PECVD-PVD, SiO₂/Mg/Ag ESC deposition by thermal evaporation, spin coating of the conductive CNT:Nafion (a trademark polymer from DuPont) passivating contact layer, and patterned electrodes for c-PC by thermal evaporation. Two hard mask alignments are employed to form the interdigitated electron-selective contact strip (SiO₂/Mg/Ag) and the electrode strip

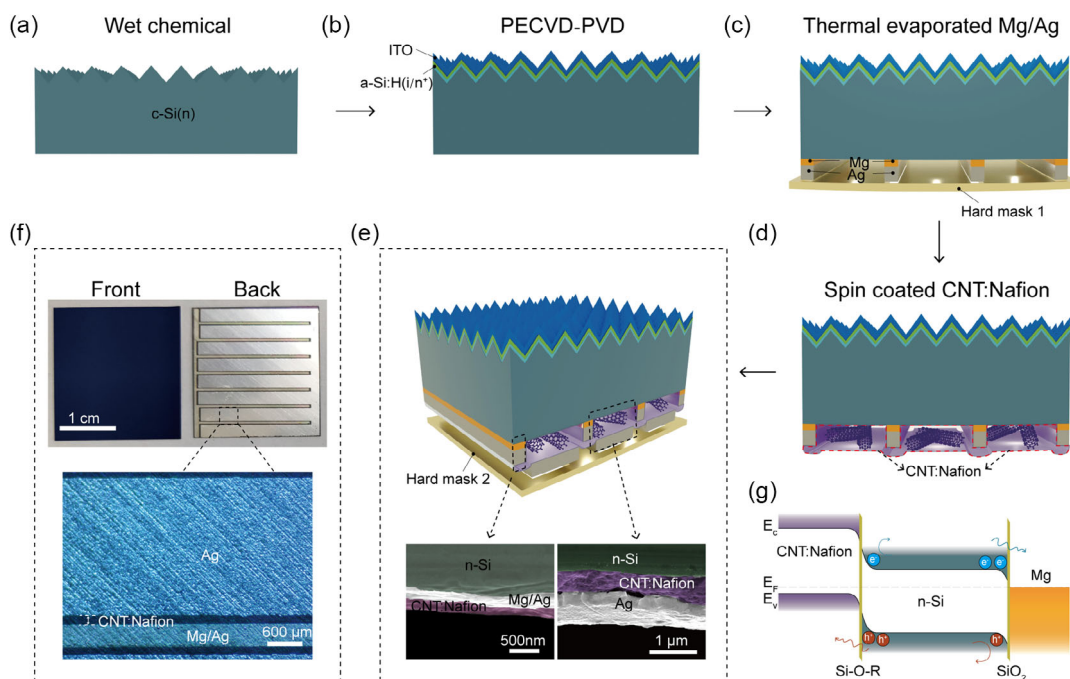


Figure 1. The IBC-CNT solar cell concept and its low-complexity fabrication process. a–f) Cross-sectional schematics of the IBC-CNT solar cell showing the required fabrication steps. (a) Wet-chemical texturing and planarizing the rear of the wafer. (b) Front surface passivation and antireflection using a-Si:H and ITO. (c) Patterned SiO₂/Mg/Ag ESC deposition by thermal evaporation using in situ shadow masking. (d) Full-area CNT:Nafion film coating to a conductive passivating contact. (e) Patterned electrodes on the CNT:Nafion film via an aligned masking and corresponding SEM images of the back contact regions. (f) Photograph of the back and front of the solar cell and a microscope enlargement for an unit, including HSC, gap, and ESC region. (g) Sketch of the band alignment of the cell showing its predicted work principle.

containing the CNTs. One of key technologies required to realize the IBC-CNT cells was passivation of the back surface defects at the ESC strip region. This was performed by the SiO₂/Mg stack layer; specifically, passivation of the back surface defects at the hole-selective contact (HSC) strip and the gap (between the n- and p- contact strips) region is achieved by the composite CNT:Nafion thin film. This film is also hole selective. The technological scheme presented here omits the vacuum-fabricated a-Si:H passivation layer used in the usual dopant-free IBC cells, but to focus on the backside the front side of the IBC-CNT cells was still fabricated in the traditional manner with a pyramid-textured structure covered by the conventional ITO/a-Si:H thin films (Figure 1b).

The CNT film is a random network of nanotube alignment directions and directly coating the CNT ink onto highly rough pyramid surface that led to poor surface coverage.^[50,51] Thus, the back surface needed to be nearly planarized for a better coverage of the CNT layer and to ensure the formation of a good emitter/junction. This was essential to high performance.^[50] Before deposition of the Mg layer, an ultrathin SiO₂ layer (≈1 nm) was natively grown for 1 h by exposing the wafer to oxygen according to the method reported in previous work.^[56] The dual function of tailoring heterojunction lineup while maintaining surface passivation for the silicon oxide/magnesium has been demonstrated by the previous work,^[57] and here we also found that this interfacial oxide is helpful to improve the open circuit voltage (V_{oc}) and fill factor (FF) (Figure S1, Supporting Information) of the IBC-CNT cells because its addition separates the direct contact between the metal Mg and semiconductor Si surface and reduces defect-assisted Shockley–Read–Hall contact

recombination. Following the mask, a ≈50 nm Mg thin film was fabricated on the interfacial layer and subsequently a ≈300 nm Ag layer is added on the top of Mg. This layer protects the easily oxidized Mg and also prevents corrosion by the CNT:Nafion layer (Figure 1c). The CNT:Nafion thin film was spin coated on the total back surface, including Mg/Ag region by using a CNT:Nafion ink (Figure 1d).^[51] Here, Nafion is responsible for the passivation of surface defects and CNT is responsible for the formation the CNT/Si HJ as separator of electron–hole pairs (i.e., so-called emitter or HSC). The CNT:Nafion ratio is optimized to be 2 mg mL⁻¹, as shown in Figure S2, Supporting Information. A final IBC-CNT cell is achieved by metallization of a patterned comb, which defines the emitter of the CNT:Nafion/patterned Ag and the gap between the emitter and the Mg/Ag ESC (Figure 1e).

Figure 1e shows a cross-sectional scanning electron microscope (SEM) image of the rear side of the IBC-CNT cell. It can be clearly seen that the CNT:Nafion contacted the Si in the C/Si HJ and gap region and wrapped up the Mg/Ag ESC by directly covering the Mg/Ag patterns. A photograph of the front and back of the solar cell and a microscope enlargement for HSC and ESC pattern is shown in Figure 1f. The principle of operation of the device is shown in Figure 1g. An optimized gap of ≈150 μm was obtained by studying the photovoltaic parameters of the cell with different gap sizes (Figure S3, Supporting Information). Isolation of two contact polarities is achieved by low conductance of the CNT:Nafion thin film. Here, we used CoMoCAT (6, 5) CNTs, which are semiconducting and have poor transversal conductivity. The CNTs are

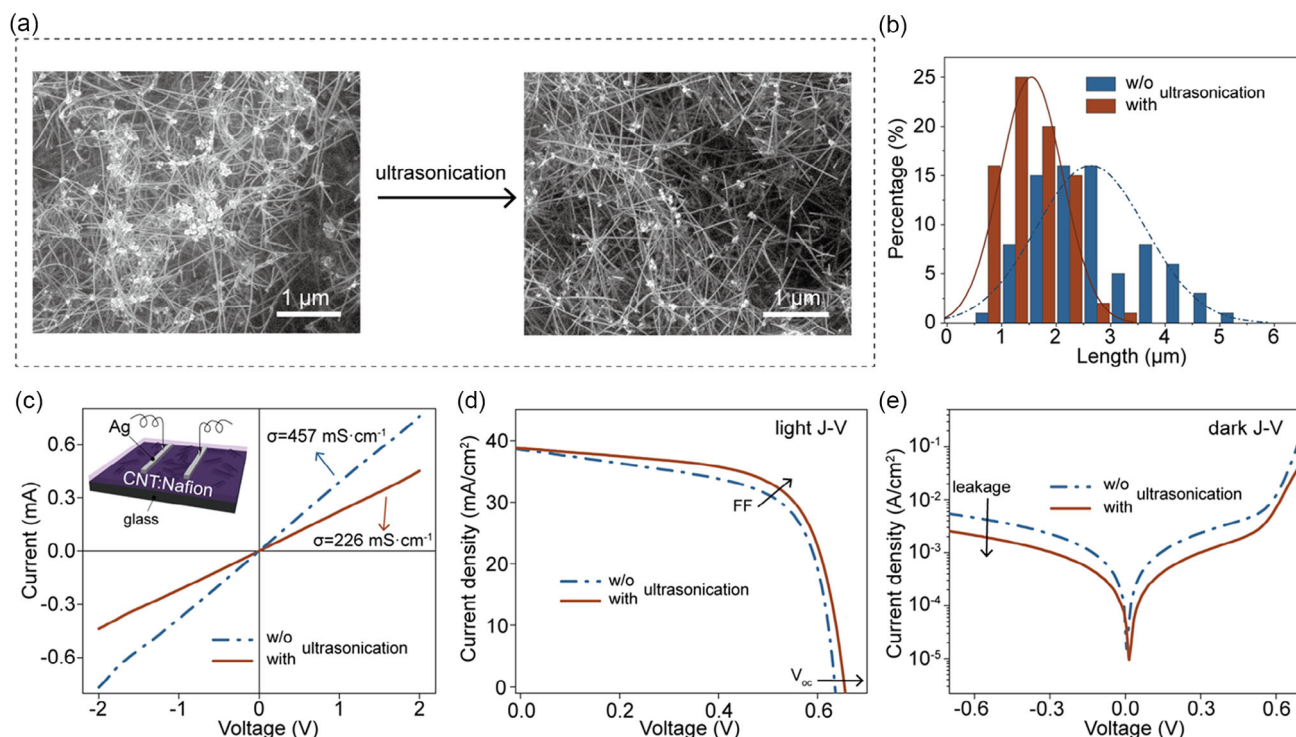


Figure 2. The used low-conductivity CoMoCAT (6, 5) CNT films and its device performances. a) SEM images of the CNT:Nafion films with and without ultrasonication of the precursor solution. b) Length distributions of the CNTs or their bundles from SEM analysis. c) Conductivity measurement using a Ag coplanar electrode configuration. d,e) Light and dark current–voltage curves of the IBC-CNT cells, with and without ultrasonicated CNTs.

commercially available under the names SG65i, which are cost-effective and have been proved to be able to achieve industrial CNT–silicon solar cells with an efficiency exceeding 23%.^[52]

The absorption spectroscopy of the materials is seen in Figure S4, Supporting Information. It is found that ultrasonication of the CNT:Nafion leads to a lower conductivity than its pristine state (Figure 2a) due to the reduction of the length of the nanotubes or their bundles and the reduced possibility of kinking (Figure 2b). This results in lower leakage current (Figure 2c) and thus better FF and V_{oc} of the IBC-CNT cell (Figure 2d). As the CNT films were placed on the rear side of the cells, the electrical properties of the CNT in the IBC-CNT cells can be separately optimized without compromise of the optical properties.

It is found that the external quantum efficiency (EQE) of the IBC-CNT cells was dependent on the position of measurement (Figure 3a). Specifically, there was a large difference in the EQE

curves between the ESC (SiO₂/Mg), gap and HSC (CNT:Nafion) regions (Figure 3b). This is related to a kind of the electrical shading loss, which is caused by a reduced carrier collection probability associated with the recombination at the base region rear side and the extended lateral path of the minority carriers generated above the base region from ESC to HSC.^[58,59] This electrical shading leads to the short-circuit current densities (J_{sc}) measured from the EQE curves and current density–voltage (J – V) curves being completely different. The difference, $\Delta J = J_{sc}(\text{EQE}) - J_{sc}(J-V)$, is highly sensitive to the width and surface recombination velocity of the HSC and ESC regions and the gaps between them. EQE is high at the CNT:Nafion HSC region, medium at the gap region, and low at the SiO₂/Mg ESC region (Figure 3b). We found that the CNT-HSC coverage area fraction (f_{CNT}), which is defined as the ratio between the electrode area on the CNT:Nafion (emitter width) and the CNT:Nafion plus ESC

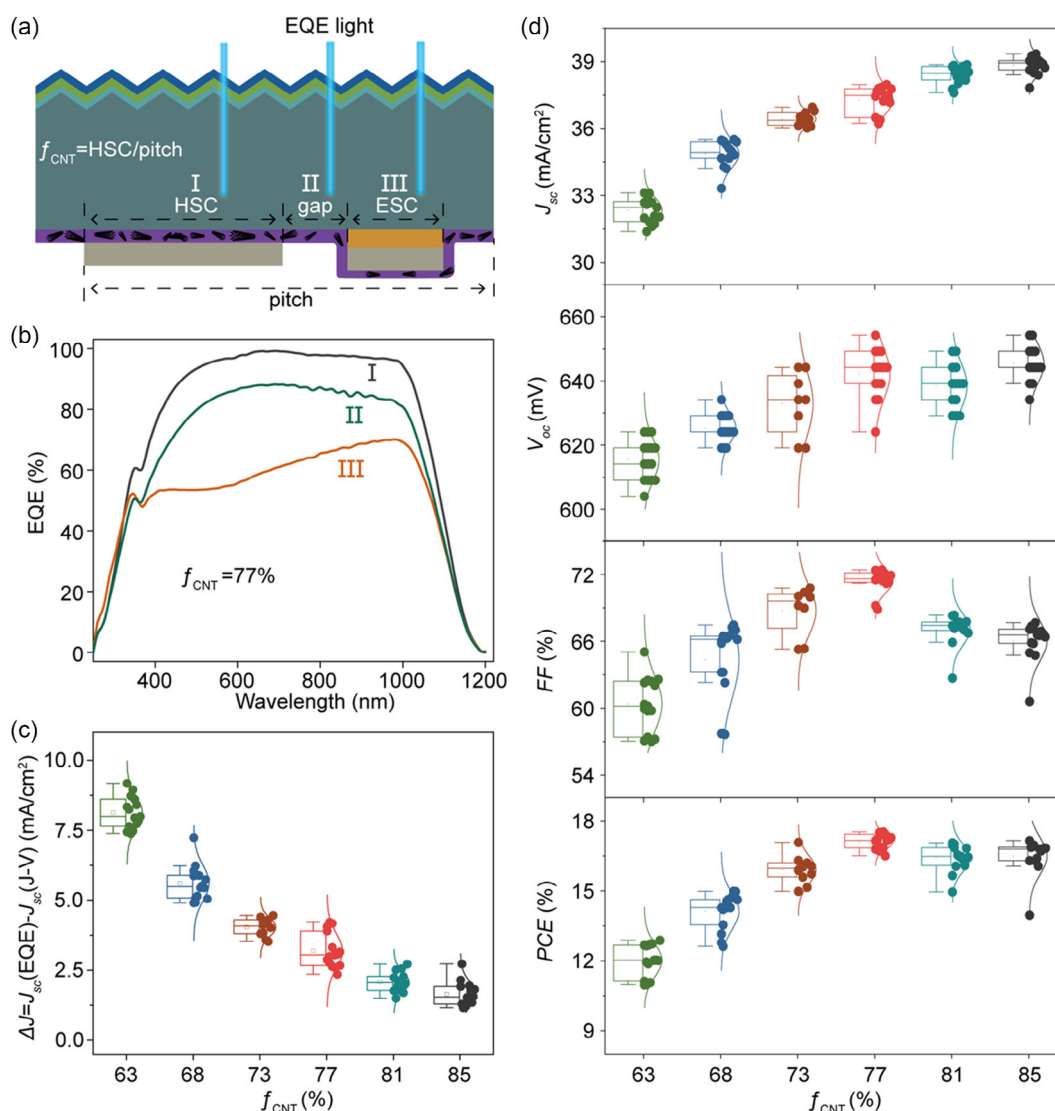


Figure 3. The EQE and photovoltaic parameters as function of the CNT-HSC coverage area fraction (f_{CNT}). a) EQE measuring schemes, corresponding different measuring points at the ESC (SiO₂/Mg), gap, and HSC (CNT:Nafion) regions. b) Measured EQE curves with a $f_{\text{CNT}} = 77\%$. c) The difference $\Delta J = J_{sc}(\text{EQE}) - J_{sc}(J-V)$ and d) Photovoltaic parameters, including J_{sc} , V_{oc} , FF, and PCE, as function of the f_{CNT} .

area, is an important factor for reducing ΔJ . As shown in Figure 3c, ΔJ can be decreased to ≈ 1 from $\approx 8 \text{ mA cm}^{-2}$, which corresponds to the improved J_{sc} (J - V) and V_{oc} of the IBC-CNT cells (Figure 3d). This improvement resulted mainly from an increased effective surface passivation of the gap and C/Si HJ by the CNT:Nafion films. However, with further increase of f_{CNT} , the emitter region becomes larger, the lateral path of the minority carriers is extended, and this results in a higher series resistance and a reduction in FF. An optimized value of f_{CNT} was 77% (i.e., CNT:Nafion, 2 500 μm and Ag on the top of CNT: Nafion, 2 200 μm ; SiO_2/Mg , 350 μm ; gap, 150 μm), and a champion device with a PCE of 17.53% was obtained. This corresponded to a V_{oc} of 651 mV, J_{sc} of 37.7 mA cm^{-2} , and FF of 71.6% (Figure 4a). Here, note that the entire wafer is used as the active area and then a large device area of 4.76 cm^2 is achieved. This reproducibility is enabled by accurate alignment of interdigitated electrodes, stable back surface wet chemistry, and the preparation of the ink with the accurate CNT:Nafion ratio.

The respectable V_{oc} of the IBC-CNT cell benefited from the excellent passivation of Nafion on a large portion of the rear surface. However, there is still potential to improve the performance of these cells. A Suns- V_{oc} measurement was employed to evaluate the potential FF without the series resistance,^[60] and a

so-called pseudo FF (pFF) of up to 81.33% was obtained. Combining this FF with the best J_{sc} (EQE), an efficiency exceeding 21.39% can be predicted on this kind of simple IBC-CNT cells. Further improvement for the IBC-CNT performance may be possible by developing efficient low work function ESCs that are compatible with the current processes. For example, it is possible to use a high-quality ultrathin passivation layer as alternative of the current native SiO_2 layer. Furthermore, an aligned CNT film may be beneficial in reducing lateral leakage and increasing V_{oc} and FF.

In conclusion, we have demonstrated an IBC-CNT solar cell concept with conductive hole-selective passivating contacts and a simple design. The formation of the IBC pattern and alignment was photolithographic-free and involved in room-temperature processing. A CNT ratio (f_{CNT}) of 77% corresponding to CNT: Nafion of 2 200 μm , SiO_2/Mg of 350 μm , and gap of 150 μm was shown to be optimal and minimized the electrical shading loss and improved the photocarrier collection probability. Large-area (4.76 cm^2) highly efficient (17.53%) device was demonstrated with a V_{oc} of 651 mV and J_{sc} of 40.56 mA cm^{-2} . These results are first reported for an IBC CNT/Si solar cells and are among the best for solution-processed dopant-free IBC schemes. The novel IBC-CNT cells not only developed the simple architecture and fabrication of back-contacted solar cells, but also revealed the advantages of the organic-passivated CNT films with excellent passivation, hole selectivity, and low lateral conductivity simultaneously. This work demonstrates a feasibility of using low-D carbon materials to exploit IBC C/Si HJ solar cells as a very promising design.

2. Experimental Section

Solution Preparation: A Nafion solution with 10% water content was obtained by mixing an original 20 wt% Nafion (Sigma-Aldrich, 20 wt% in a mixture of lower aliphatic alcohols and 34% water) with ethanol (Sigma-Aldrich, 20 proof, anhydrous, $\geq 99.5\%$). Simple magnetic stirring for at least 6 h was used to obtain a uniform precursor solution. The CNT: Nafion composite solution was prepared by ultrasonic 3 min after dispersing SG65i SWCNT (Sigma-Aldrich, $\geq 95\%$) with Nafion solution in the ratio of 2 mg mL^{-1} by shear force mixing for 3 h to ensure the good reproducibility of device performances. The CNT:Nafion composite thin films were spin coated at 5 000 rpm for 60 s.

IBC-CNT Solar Cells: The solar cell was fabricated using an (100)-oriented n-type CZ wafers with a thickness of about 180 μm , a resistivity of about $2 \Omega \text{ cm}$, and bulk-doping concentration of about $2.4 \times 10^{15} \text{ cm}^{-3}$. Device fabrication involves steps: 1) wet chemistry, including texturing, back surface smoothing, and cleaning of wafer surfaces with the method found elsewhere using the KOH solution and a mixed $\text{HNO}_3/\text{HF}/\text{H}_2\text{O}$ (4:1:2) solution, which was highly associated with achieving high-performance repeatability; 2) the formation of the front electron-selective passivating contact, a-Si:H (i/n^+) stack layer was deposited using a plasma-enhanced chemical vapor deposited (PECVD) equipment on the textured front surface of n-type wafers, and then a ITO layer was deposited by magnetron sputtering on the top of the a-Si:H (i/n^+); 3) the polished surface of n-type wafers is fixed on the hard mask 1 and placed in the oxygen chamber for 10 min to form an ultrathin SiO_2 layer and then a thermal evaporation was used to deposit Mg (50 nm)/Ag (300 nm) through the shielding of mask 1 as an ESC; 4) spin coating of CNT: Nafion thin film on back side at 5 000 rpm under N_2 atmosphere at room temperature; and 5) then, alignment of hard mask 2 and thermal evaporation of the HSC electrodes. Repeatability is achieved by good alignment of the interdigitated electrodes.

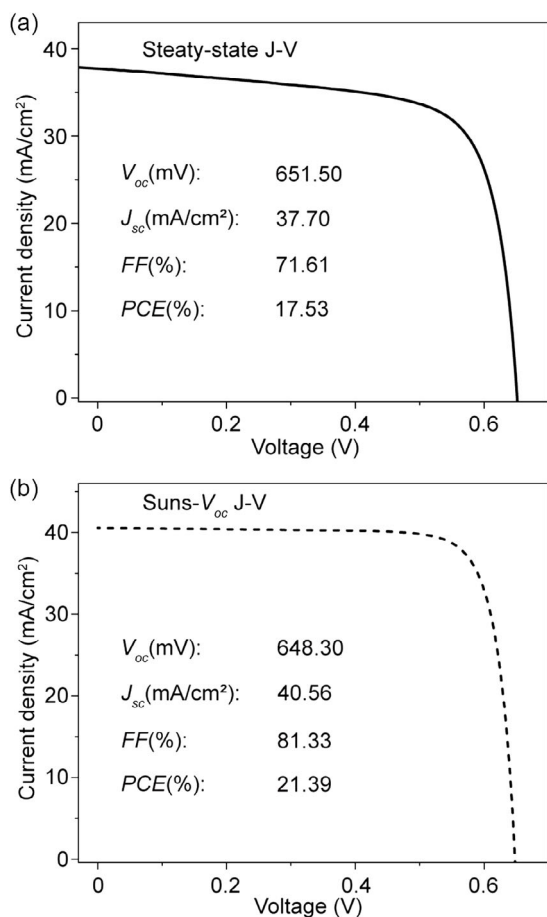


Figure 4. Champion IBC-CNT solar cell. a) 1 sun J - V characteristic and b) Suns- V_{oc} measurement.

Characterization: The surface morphologies of the samples were observed by scanning electron microscopy (SEM) (Nova Nano Sem450, FEI) and light microscope (SDPTOP). Solar cells were characterized by current density–voltage (J – V) measurements under standard test conditions (AM 1.5 100 mW cm⁻², and 25 °C) and the EQE (R3011, Enlitech). The current versus voltage (J – V) measurements were carried out with a semiconductor device analyzer (Agilent, B1500A). J – V measurements were conducted using a solar simulator (SAN-EIXES-100S1, level AAA) and a SYSTEM SourceMeter (Keithley 2601B). The light source was calibrated by Reference Solar Cell (RS-ID4, Ser. No.076-2014) from Fraunhofer ISE before measuring the device.

Supporting Information

Supporting Information is available from the Wiley Online Library or from the author.

Acknowledgements

We gratefully acknowledge support from the National Natural Science Foundation of China (62274054), the Hebei Province Science Foundation for Distinguished Young Scholars (F2021201035), “333 project” of Hebei Province (C20221014), the Central Guidance on Local Science and Technology Development Fund Project of Hebei Province (grant no. 226Z4306G), the Outstanding Youth Science Foundation of Hebei Province (F2019201367), the Top Young Outstanding Innovative Talents Program of Hebei Province (BJ2021006), the National Program on Key R&D of China (2018YFB1500201), the Key Research and Development Program of Hebei Province (grant no. 20314305D), the Natural Science Foundation of Hebei Province (F2019204325), and the cooperative scientific research project of “Chunhui Program” of Ministry of Education (2018-7). B.S.F. and H.L. gratefully acknowledge support from the Deutsche Forschungsgemeinschaft (DFG) under grant numbers FL 834/5-1, FL 834/7-1, FL 834/9-1, and FL 834/12-1.

Conflict of Interest

The authors declare no conflict of interest.

Data Availability Statement

The data that support the findings of this study are available in the supplementary material of this article.

Keywords

carbon nanotubes, heterojunctions, interdigitated back contacts, solar cells

Received: December 6, 2022

Revised: February 1, 2023

Published online:

- [1] N. Pirrone, F. Bella, S. Hernández, *Green Chem.* **2022**, *24*, 5379.
- [2] K. Masuko, M. Shigematsu, T. Hashiguchi, D. Fujishima, M. Kai, N. Yoshimura, T. Yamaguchi, Y. Ichihashi, T. Mishima, N. Matsubara, *IEEE J. Photovoltaics* **2014**, *4*, 1433.
- [3] T. Feurer, P. Reinhard, E. Avancini, B. Bissig, J. Löckinger, P. Fuchs, R. Carron, T. P. Weiss, J. Perrenoud, S. Stutterheim, *Prog. Photovoltaics Res. Appl.* **2017**, *25*, 645.

- [4] F. Schmitz, N. Lago, L. Fagiolari, J. Burkhart, A. Cester, A. Polo, M. Prato, G. Meneghesso, S. Gross, F. Bella, *ChemSusChem* **2022**, *15*, e202201590.
- [5] N. Cheng, Z. Liu, W. Li, Z. Yu, B. Lei, W. Zi, Z. Xiao, S. Sun, Z. Zhao, P.-A. Zong, *Chem. Eng. J.* **2023**, *454*, 140146.
- [6] D. Cao, Z. Li, Y. Xu, W. Li, H. Zhong, Y. Huang, X. Zhang, L. Wan, X. Zhang, Y. Li, *Org. Electron.* **2023**, *113*, 106699.
- [7] T. M. W. J. Bandara, J. M. C. Hansadi, F. Bella, *Ionics* **2022**, *28*, 2563.
- [8] M. Bonomo, A. S. Zarate, L. Fagiolari, A. Damin, S. Galliano, C. Gerbaldi, F. Bella, C. Barolo, *Mater. Today Sustainability* **2023**, *21*, 100271.
- [9] Y. Liu, Y. Li, Y. Wu, G. Yang, L. Mazzarella, P. Procel-Moya, A. C. Tamboli, K. Weber, M. Boccard, O. Isabella, X. Yang, B. Sun, *Mater. Sci. Eng.: R: Rep.* **2020**, *142*, 100579.
- [10] K. Yoshikawa, H. Kawasaki, W. Yoshida, T. Irie, K. Konishi, K. Nakano, T. Uto, D. Adachi, M. Kanematsu, H. Uzu, K. Yamamoto, *Nat. Energy* **2017**, *2*, 17032.
- [11] NREL, **2022**, <https://www.nrel.gov/pv/cell> (accessed: November 2022).
- [12] J. Haschke, O. Dupré, M. Boccard, C. Ballif, *Sol. Energy Mater. Sol. Cells* **2018**, *187*, 140.
- [13] M. Bivour, J. Temmler, H. Steinkemper, M. Hermle, *Sol. Energy Mater. Sol. Cells* **2015**, *142*, 34.
- [14] J. Geissbühler, J. Werner, S. Martin de Nicolas, L. Barraud, A. Hessler-Wyser, M. Despeisse, S. Nicolay, A. Tomasi, B. Niesen, S. De Wolf, *Appl. Phys. Lett.* **2015**, *107*, 081601.
- [15] C. Battaglia, S. M. De Nicolas, S. De Wolf, X. Yin, M. Zheng, C. Ballif, A. Javey, *Appl. Phys. Lett.* **2014**, *104*, 113902.
- [16] J. Dréon, Q. Jeangros, J. Cattin, J. Haschke, L. Antognini, C. Ballif, M. Boccard, *Nano Energy* **2020**, *70*, 104495.
- [17] Y. Han, Y. Liu, J. Yuan, H. Dong, Y. Li, W. Ma, S.-T. Lee, B. Sun, *ACS Nano* **2017**, *11*, 7215.
- [18] J. P. Thomas, K. T. Leung, *Adv. Funct. Mater.* **2014**, *24*, 4978.
- [19] S. Avasthi, S. Lee, Y. L. Loo, J. C. Sturm, *Adv. Mater.* **2011**, *23*, 5762.
- [20] S. Jäckle, M. Mattiza, M. Liebhaber, G. Brönstrup, M. Rommel, K. Lips, S. Christiansen, *Sci. Rep.* **2015**, *5*, 1.
- [21] H. C. Fu, V. Ramalingam, H. Kim, C. H. Lin, X. Fang, H. N. Alshareef, J. H. He, *Adv. Mater.* **2019**, *9*, 1900180.
- [22] X. H. An, F. Z. Liu, S. Kar, *Carbon* **2013**, *57*, 329.
- [23] X. M. Li, Z. Lv, H. W. Zhu, *Adv. Mater.* **2015**, *27*, 6549.
- [24] Y. Jia, J. Q. Wei, K. L. Wang, A. Y. Cao, Q. K. Shu, X. C. Gui, Y. Q. Zhu, D. M. Zhuang, G. Zhang, B. B. Ma, L. D. Wang, W. J. Liu, Z. C. Wang, J. B. Luo, D. Wu, *Adv. Mater.* **2008**, *20*, 4594.
- [25] N. Martín, *Adv. Mater.* **2017**, *7*, 1601102.
- [26] A. S. Bati, L. Yu, M. Batmunkh, J. G. Shapter, *Adv. Funct. Mater.* **2019**, *29*, 1902273.
- [27] N. M. Gabor, Z. Zhong, K. Bosnick, J. Park, P. L. McEuen, *Science* **2009**, *325*, 1367.
- [28] S. Wang, M. Khafizov, X. Tu, M. Zheng, T. D. Krauss, *Nano Lett.* **2010**, *10*, 2381.
- [29] S. Konabe, S. Okada, *Phys. Rev. Lett.* **2012**, *108*, 227401.
- [30] K. Mizuno, J. Ishii, H. Kishida, Y. Hayamizu, S. Yasuda, D. N. Futaba, M. Yumura, K. Hata, *Proc. Natl. Acad. Sci.* **2009**, *106*, 6044.
- [31] S. Evlashin, S. Svyakhovskiy, N. Suetin, A. Pilevsky, T. Murzina, N. Novikova, A. Stepanov, A. Egorov, A. Rakhimov, *Carbon* **2014**, *70*, 111.
- [32] V. Krivchenko, S. Evlashin, K. Mironovich, N. Verbitskiy, A. Nefedov, C. Wöll, A. Y. Kozmenkova, N. Suetin, S. Svyakhovskiy, D. Vyalikh, *Sci. Rep.* **2013**, *3*, 1.
- [33] Y. Miyata, K. Shiozawa, Y. Asada, Y. Ohno, R. Kitaura, T. Mizutani, H. Shinohara, *Nano Res.* **2011**, *4*, 963.
- [34] E. Snow, P. Campbell, M. Ancona, J. Novak, *Appl. Phys. Lett.* **2005**, *86*, 033105.

- [35] C.-K. Liu, H.-L. Loi, J. Cao, G. Tang, F. Liu, Q. Huang, X. Liang, F. Yan, *Small Struct.* **2021**, *2*, 2000084.
- [36] M. H. Yun, J. W. Kim, S. Y. Park, D. S. Kim, B. Walker, J. Y. Kim, *J. Mater. Chem. A* **2016**, *4*, 16410.
- [37] S. H. Ju, B. X. Liang, J. Z. Wang, Y. Shi, S. L. Li, *Opt. Commun.* **2018**, *428*, 258.
- [38] G. F. Fan, H. W. Zhu, K. L. Wang, J. Q. Wei, X. M. Li, Q. K. Shu, N. Guo, D. H. Wu, *ACS Appl. Mater. Interfaces* **2011**, *3*, 721.
- [39] Q. Gao, J. Yan, L. Wan, C. Zhang, Z. Wen, X. Zhou, H. Li, F. Li, J. Chen, J. Guo, *Adv. Mater. Interfaces* **2022**, *9*, 2201221.
- [40] J. M. Harris, M. R. Semler, S. May, J. A. Fagan, E. K. Hobbie, *J. Phys. Chem. C* **2015**, *119*, 10295.
- [41] P. Wadhwa, B. Liu, M. A. McCarthy, Z. Wu, A. G. Rinzler, *Nano Lett.* **2010**, *10*, 5001.
- [42] Z. Li, V. P. Kunets, V. Saini, Y. Xu, E. Dervishi, G. J. Salamo, A. R. Biris, A. S. Biris, *ACS Nano* **2009**, *3*, 1407.
- [43] Y. Jung, X. Li, N. K. Rajan, A. D. Taylor, M. A. Reed, *Nano Lett.* **2013**, *13*, 95.
- [44] J. Wei, Y. Jia, Q. Shu, Z. Gu, K. Wang, D. Zhuang, G. Zhang, Z. Wang, J. Luo, A. Cao, *Nano Lett.* **2007**, *7*, 2317.
- [45] X. Li, Y. Jung, K. Sakimoto, T.-H. Goh, M. A. Reed, A. D. Taylor, *Energy Environ. Sci.* **2013**, *6*, 879.
- [46] F. Wang, D. Kozawa, Y. Miyauchi, K. Hiraoka, S. Mouri, Y. Ohno, K. Matsuda, *Nat. Commun.* **2015**, *6*, 1.
- [47] K. Cui, Y. Qian, I. Jeon, A. Anisimov, Y. Matsuo, E. I. Kauppinen, S. Maruyama, *Adv. Mater.* **2017**, *7*, 1700449.
- [48] X.-G. Hu, P.-X. Hou, C. Liu, F. Zhang, G. Liu, H.-M. Cheng, *Nano Energy* **2018**, *50*, 521.
- [49] Y. Qian, I. Jeon, Y. L. Ho, C. Lee, S. Jeong, C. Delacou, S. Seo, A. Anisimov, E. I. Kauppinen, Y. Matsuo, *Adv. Mater.* **2020**, *10*, 1902389.
- [50] J. Yan, C. Zhang, H. Li, X. Yang, L. Wan, F. Li, K. Qiu, J. Guo, W. Duan, A. Lambertz, *Adv. Sci.* **2021**, *8*, 2102027.
- [51] J. Chen, L. Wan, H. Li, J. Yan, J. Ma, B. Sun, F. Li, B. S. Flavel, *Adv. Funct. Mater.* **2020**, *30*, 2004476.
- [52] Q. Gao, J. Yan, H. Li, J. Chen, X. Yang, Y. Bai, X. Zhang, B. Chen, J. Guo, W. Duan, K. Han, F. Li, J. Wang, D. Song, S. Wang, B. S. Flavel, J. Chen, *Carbon* **2023**, *202*, 432.
- [53] F. Haase, C. Hollemann, S. Schafer, A. Merkle, M. Rienacker, J. Krugener, R. Brendel, R. Peibst, *Sol. Energy Mater. Sol. Cells* **2018**, *186*, 184.
- [54] K. Yoshikawa, W. Yoshida, T. Irie, H. Kawasaki, K. Konishi, H. Ishibashi, T. Asatani, D. Adachi, M. Kanematsu, H. Uzu, K. Yamamoto, *Sol. Energy Mater. Sol. Cells* **2017**, *173*, 37.
- [55] N. Mingirulli, J. Haschke, R. Gogolin, R. Ferre, T. F. Schulze, J. Dusterhoft, N. P. Harder, L. Korte, R. Brendel, B. Rech, *Phys. Status Solidi RRL* **2011**, *5*, 159.
- [56] Y. Song, X. Li, C. Mackin, X. Zhang, W. Fang, T. Palacios, H. Zhu, J. Kong, *Nano Lett.* **2015**, *15*, 2104.
- [57] H. Tong, Z. Yang, X. Wang, Z. Liu, Z. Chen, X. Ke, M. Sui, J. Tang, T. Yu, Z. Ge, *Adv. Mater.* **2018**, *8*, 1702921.
- [58] S. Kluska, F. Granek, M. Rüdiger, M. Hermle, S. W. Glunz, *Sol. Energy Mater. Sol. Cells* **2010**, *94*, 568.
- [59] C. Reichel, F. Granek, M. Hermle, S. Glunz, *J. Appl. Phys.* **2011**, *109*, 024507.
- [60] T. Roth, J. Hohl-Ebinger, D. Grote, E. Schmich, W. Warta, S. W. Glunz, R. A. Sinton, *Rev. Sci. Instrum.* **2009**, *80*, 033106.